3D PRINTING AND ADDITIVE MANUFACTURING
Volume 11, Number 1, 2024

DOI: 10.1089/3dp.2021.0228

ORIGINAL ARTICLE

Laser Powder Bed Fusion of Sm-Fe-N Bonded Magnets Employing Flake Powders

Melissa Röhrig,[1] Rafael Gitti Tortoretto Fim,[1] Rubens Nunes de Faria Júnior,[2] Cristiani Campos Plá Cid,[1] Carlos Henrique Ahrens,[1] and Paulo Wendhausen[1]

Abstract

In this work, the role of the binder volumetric fraction used on the consolidation process of Sm-Fe-N-based bonded magnets obtained *via* the laser powder bed fusion technique has been investigated and explained. The magnetic samples have been obtained *via* the Selective Laser Sintering (SLS) process, using a mixture of polyamide-12 powder (PA12, DuraForm PA2200) and isotropic Sm-Fe-N melt-spun ribbons (Daido Electronics, Inc.) as feedstocks. The binder content has been varied between 34% and 65% vol. Geometrical density values increased systematically as the PA12 content was increased, reaching a maximum value of $\rho = 3.35\ g/cm^3$ (60% vol.), which represents 89% of a fully dense composite. In this composition, the maximum magnetic properties values have been achieved, $J_r = 369$ mT and $(BH)_{max} = 24\ kJ/m^3$. A further increase on the PA12 fraction up to 65% vol. resulted on magnetic samples with 97% relative density, but at the expense of magnetic performance. The formation of a continuous polymeric matrix has been observed *via* Scanning Electron Microscopy (SEM) analysis when PA12 fraction was on the interval between 60% and 65% vol., not observable for the other explored conditions. Volumetric binder fractions comparable with other published works, which used spherical particles as raw materials for feedstock production, showed inadequate consolidation and required adjustments for proper densification.

Keywords: additive manufacturing, bonded magnets, Sm-Fe-N magnets, laser powder bed fusion (LPBF)

Introduction

Additive manufacturing (AM) of rare earth bonded magnets has been described and presented as a potential manufacturing route to obtain complex net-shape parts with promising performance. Several researchers have been using Nd-Fe-B-based compounds as the main hard magnetic phase for AM processes,[1–8] with limited exploration of alternative magnetic systems, such as Sm-Fe-N, for example.[9,10]

Commercial powders based on the $SmFe_7N_x$ phase present comparable magnetic properties with the well-known counterpart $Nd_2Fe_{14}B$ phase, such as anisotropy field (H_A: $SmFe_7N_x = 4.7$ T; $Nd_2Fe_{14}B = 7.5$ T), saturation polarization (J_s: $SmFe_7N_x = 1.54$ T; $Nd_2Fe_{14}B = 1.64$ T), superior Curie temperature (T_c: $SmFe_7N_x = 470°C$; $Nd_2Fe_{14}B = 316°C$), corrosion, and aging resistance.[11,12] Furthermore, this magnetic system is metastable at temperatures above 600°C, where conventional sintering processes cannot be applicable, making it a suitable candidate for bonded magnet manufacturing.[11,12]

In a previous work of our group, Engerroff *et al.*[13] reported the obtention of isotropic Sm-Fe-N-based bonded magnets *via* the Laser Powder Bed Fusion (LPBF) technique. In their work, a mixture of $SmFe_7N_x$ melt-spun ribbons (Nitroquench-P grade) and 34% vol. of PA12 powder (InnovPA 1550 XS grade) was used as feedstock and processed into magnetic samples. The as-printed magnetic samples exhibited a maximum geometrical density value of $\rho = 2.48\ g/cm^3$ for all combinations explored, which is very close to the apparent density (AD) of the feedstock ($AD = 2.32–2.35\ g/cm^3$).

Those values represent a porosity level of 54% that was only reduced after a cold isostatic pressing cycle, showing the poor consolidation level obtained during the LPBF. The obtained results showed that the porosity was insensitive to the processing conditions explored, making it possible to associate the elevated porosity degree with feedstock characteristics.

The porosity values of the as-printed magnets presented by Engerroff *et al.* were superior to those reported by Baldissera

[1]Mechanical Engineering Department, Federal University of Santa Catarina, Florianopolis, Brazil.
[2]Metallurgy Department, Energy and Nuclear Research Institute, IPEN-CNEN, São Paulo, Brazil.

et al.,[14] which investigated the obtention of Nd-Fe-B-bonded magnets *via* LPBF using a spherical powder as raw material for feedstock production. Under similar processing conditions and using a feedstock with the same composition (34% vol. PA12), the obtained as-printed magnets presented geometrical density values of $\rho = 3.60\ g/cm^3$, which represents 30% of porosity. This difference in porosity values suggested that consolidation was influenced by morphological characteristics of the used raw materials.

Besides particle morphology, there is also an influence of the volumetric fraction of binder used on the feedstock. Recently, Fim *et al.*[15] demonstrated the influence of PA12 volumetric fraction on the consolidation process of isotropic Nd-Fe-B bonded magnets obtained *via* LPBF. By employing feedstocks composed of 36 and 45% vol., the study investigated the influence of different PA12 fractions on the consolidation step. For the same set of processing parameters, the binder content plays a key role in the porosity elimination process, where the as-printed magnetic samples presented geometrical density values of $\rho = 4.33\ g/cm^3$ with polyamide additions up to 45% vol. These values represent 5% of porosity, leading to an increase in the overall performance of the as-printed magnetic samples.

The authors attributed these results to the adequate polyamide fraction, which enabled the formation of a continuous polymeric matrix and the elimination of porosity *via* particle rearrangement mechanism.

Although the obtention of bonded magnets *via* LPBF was reported and discussed by several authors,[13–16] the role of binder volumetric fraction has not been thoroughly investigated so far, especially when flake-shaped particles are used as raw materials for feedstock production. The reported results presented[13–16] a potential to be expanded for Sm-Fe-N bonded magnets, reinforcing the fact that the binder content on the feedstock must be adequate in the function of raw material characteristics.

Based on this context, the present work aims to clarify the influence of binder fraction on the final porosity and magnetic properties of Sm-Fe-N-based bonded magnets obtained *via* LPBF using flake-shaped powder as feedstock.

Experimental

Isotropic Sm-Fe-N bonded magnets were obtained *via* the LPBF technique using commercial Nitroquench-P grade melt-spun ribbons (Daido Electronics Co. Ltd) and DuraForm PA2200 PA12 powder (3dsystems) as raw materials for feedstock production. In this work, eight different feedstocks were produced varying the PA12 volumetric fraction between 34% and 65% *via* mechanical mixing using a Y mixer for 60 min. Originally, the Nitroquench-P powder is a melt spun ribbon flake-shaped powder with a mean particle size around 100 μm. In this investigation, the magnetic powder was comminuted and sieved between 45 and 63 μm prior to its use as feedstock. The particle size distribution (PSD) was analyzed *via* the laser diffraction technique (CILAS 1190). The physical and magnetic properties of raw materials are listed in Table 1.

Table 1. Physical and Magnetic Properties of Raw Materials Used As Feedstock[12]

Powder properties	*Nitroquench-P*	*DuraForm PA2200*
Mean particle size (μm)	45–63	50
Density (g/cm^3)	7.89	1.01
J_r (mT)	970	—
H_{cj} (kA/m)	756	—
$((BH)_{max})$ (kJ/m^3)	189	—

Table 2. Laser Powder Bed Fusion Processing Parameters[15]

Laser speed (LS)	600 mm/s
Laser power (LP)	21 W
Hatch spacing (HS)	200 μm
Layer thickness (LT)	100 μm
Printing temperature	160°C

The LPBF process was performed on Selective Laser Sintering (SLS) prototype equipment consisting of a CO_2 laser (PURI model PRR 100, $\lambda = 10.6\ \mu m$) with 100 W maximum power. For each feedstock composition, 5 cubic samples of $10 \times 10 \times 10$ mm were obtained, following the optimum processing conditions based on Fim et al.,[15] as summarized in Table 2.

Before the beginning of the laser processing, the feedstock was placed inside the feeding compartment and preheated at 160°C for 15 min using both infrared lamps and heating elements. Subsequent to the printing cycle, the magnetic samples were cooled down to room temperature prior removal from the SLS equipment. Geometrical density measurements were carried out on the as-printed magnets in order to quantify the porosity level as a function of PA12 volumetric fraction. Scanning electron microscopy (SEM; JEOL JSM-6390LV) of fracture surface from the as-printed samples was carried out in order to evaluate the resultant microstructure. Magnetic properties of the as-printed samples with the highest geometrical density values from each batch were determined *via* hysteresis measurements at room temperature using a hysteresisgraph (Brockhaus Messtechnik EM1800).

Results and Discussion

Influence of PA12 on the microstructure

Geometrical density of the as-printed magnetic samples. Table 3 summarizes the mean geometrical (ρ), theoretical (ρ_{theo}), and relative density (ρ_{rel}), as well as the porosity values of the as-printed magnetic samples as a function of PA12 volumetric fraction. It can be seen that ρ values increased systematically as the PA12 fraction increased, reaching a maximum value for the interval between 60% and 65% vol. binder, where $\rho = 3.35\ g/cm^3$ (60% vol.) and $\rho = 3.32\ g/cm^3$ (65% vol.).

The maximum achievable value for ρ in a pore-free bonded magnet (theoretical density, ρ_{theo}) can be calculated by the weighted sum of the volumetric fraction (f) of both components employed on the mixture (magnetic and polymeric powder), expressed by Eq. (1)[17] as follows:

$$\rho_{theo} = (f_{PA12} \times \rho_{PA12}) + \left(f_{Nitroquench-P} \times \rho_{Nitroquench-P}\right) \quad (1)$$

TABLE 3. MEAN GEOMETRICAL DENSITY (ρ), THEORETICAL DENSITY (ρ_{THEO}), RELATIVE DENSITY (ρ_{REL}), AND POROSITY VALUES OF THE AS-PRINTED MAGNET SAMPLES

PA12 content (vol.%)	*ρ (g/cm^3)*	*ρ_{theo} (g/cm^3)*	*ρ_{rel} (%)*	*Porosity, 100- ρ_{rel} (%)*
34	2.42 ± 0.11	5.55	44 ± 1.9	56 ± 1.9
36	2.57 ± 0.13	5.41	47 ± 2.5	53 ± 2.5
40	2.68 ± 0.01	5.14	52 ± 0.3	48 ± 0.3
45	2.77 ± 0.04	4.79	58 ± 0.8	42 ± 0.8
50	2.89 ± 0.08	4.45	65 ± 1.9	35 ± 1.9
55	3.03 ± 0.09	4.10	74 ± 2.3	26 ± 2.3
60	3.35 ± 0.03	3.76	89 ± 0.7	11 ± 0.7
65	3.32 ± 0.03	3.42	97 ± 0.8	3 ± 0.8

Thus, the relationship between the measured ρ and the ρ_{theo} is the relative density (ρ_{rel}), which represents how densified the component is.[17] The obtained values in this work show the same trend as the geometrical density, increasing with PA12 additions, starting from $\rho_{rel} = 44\%$ (34% vol. PA12) and reaching the maximum value of $\rho_{rel} = 97\%$ (65% vol. PA12). Since porosity can be estimated by 100-ρ_{rel},[17] Figure 1 presents the porosity values of the as-printed samples as a function of PA12 content.

Several factors can contribute to variations on the densification process, reflecting the final porosity level on the as-printed magnet. These factors can be mainly ascribed to feedstock characteristics in the present case since the processing parameters were kept constant:

- Technological properties of the raw materials: apparent density and flowability, particle size, size distribution, and morphology.[17–21]
- Fraction of binder employed.[15]

These results show the influence of the raw materials' technological properties on the consolidation process. Spherical particles exhibit a superior packing factor than non-spherical particles (flake-shaped particles in this case), which reflects on the initial porosity of the powder bed.[17–21]

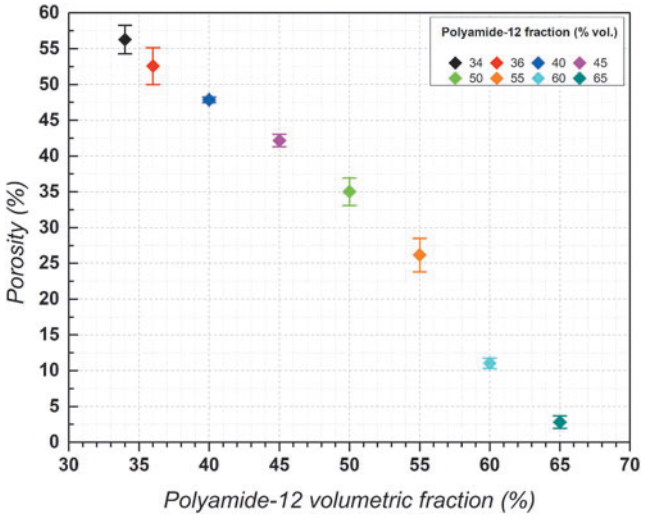

FIG. 1. Porosity values of the as-printed magnetic samples as function of PA12 volumetric fraction.

In a more packed powder bed, there are less pores to be filled by the binder,[17] then requiring less binder fraction to promote an adequate densification. As demonstrated in a previous work,[15] the porosity was reduced to 5% with PA12 additions of 45% vol., in contrast to the 65% vol., needed in this work to achieve similar values.

Due to the limited technological properties of faceted particles such as flake-shaped ones, an adequation on the binder volumetric fraction is needed to eliminate porosity. The minimum binder fraction required for this purpose is different as the particle morphology is altered, as previously reported.[13–16] For spherical Nd-Fe-B particles, the minimum binder fraction varies between 34% and 45% vol.,[14,15] resulting in as-printed samples with porosity levels of 30%[14] and 5%,[15] in this order.

In the case of flake-shaped Sm-Fe-N particles, this binder fraction falls within the range of 34% vol., generating as-printed magnetic samples with porosity of 54%.[13]

Scanning Electron Microscopy (SEM) analysis. Figure 2 presents the SEM images from the sieved magnetic powder used as raw material for feedstock production. It can be clearly seen that the particles maintained the flake-shaped morphology after the comminution step. It can also be observed a narrow particle distribution, as a result of the sieving process. PSD analysis revealed a mean particle size of 68 μm with D90 < 96 μm.

Figure 3 presents SEM images from the fracture surface of the as-printed bonded magnets obtained using 34%, 60%, and 65% vol. of PA12 fraction (see Fig. 3A–F, respectively). On the first set of images (Fig. 3A, B), it is possible to observe the presence of Sm-Fe-N flake particles (light gray), PA12 (dark gray), and pores (black areas). A detailed view, as shown on Figure 3B, presents the microstructure that is majorly formed by non-adhered Sm-Fe-N particles. The binder distribution is uneven as indicated by the arrows, accumulated in some regions with the great part of the cross section free of binder. Pores can be seen occupying a great extent on the microstructure, reinforcing the fact that there is a lack of binder in this case.

As the PA12 volumetric fraction increased, as seen in Figure 3C and D, the microstructure was drastically altered. For this feedstock composition, a continuous polymeric matrix was formed (dark gray areas) adhering the majority of the Sm-Fe-N particles. Pores can still be found on the microstructure but now more isolated, compatible with the porosity estimations presented in the previous section. In a detailed image view shown in Figure 3D, it is possible to observe a more even distribution of the binder on the microstructure, where the gaps between flake particles are completely filled.

Further PA12 additions up to 65% vol. increased even more the area occupied by the polymeric matrix, as shown in Figure 3E and F. The microstructure in this case is similar to those seen in Figure 3C and D, but now with an increase of polymeric matrix (dark gray regions) fraction. It can be seen that the gaps between particles are majorly filled by the binder, and pores are not observed on these areas, except the voids from the flake particles generated during the fracture process. This leads to a porosity reduction, as discussed earlier.

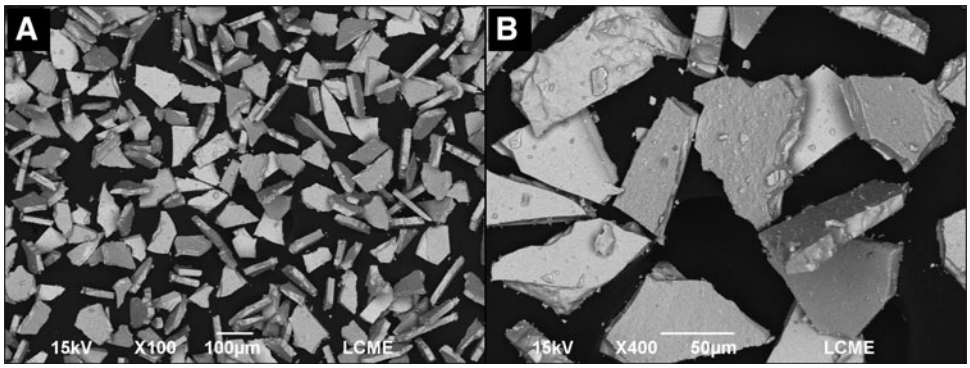

FIG. 2. SEM images from the Sm-Fe-N commercial powder used as raw material for feedstock production. **(a)** general and **(b)** detailed view.

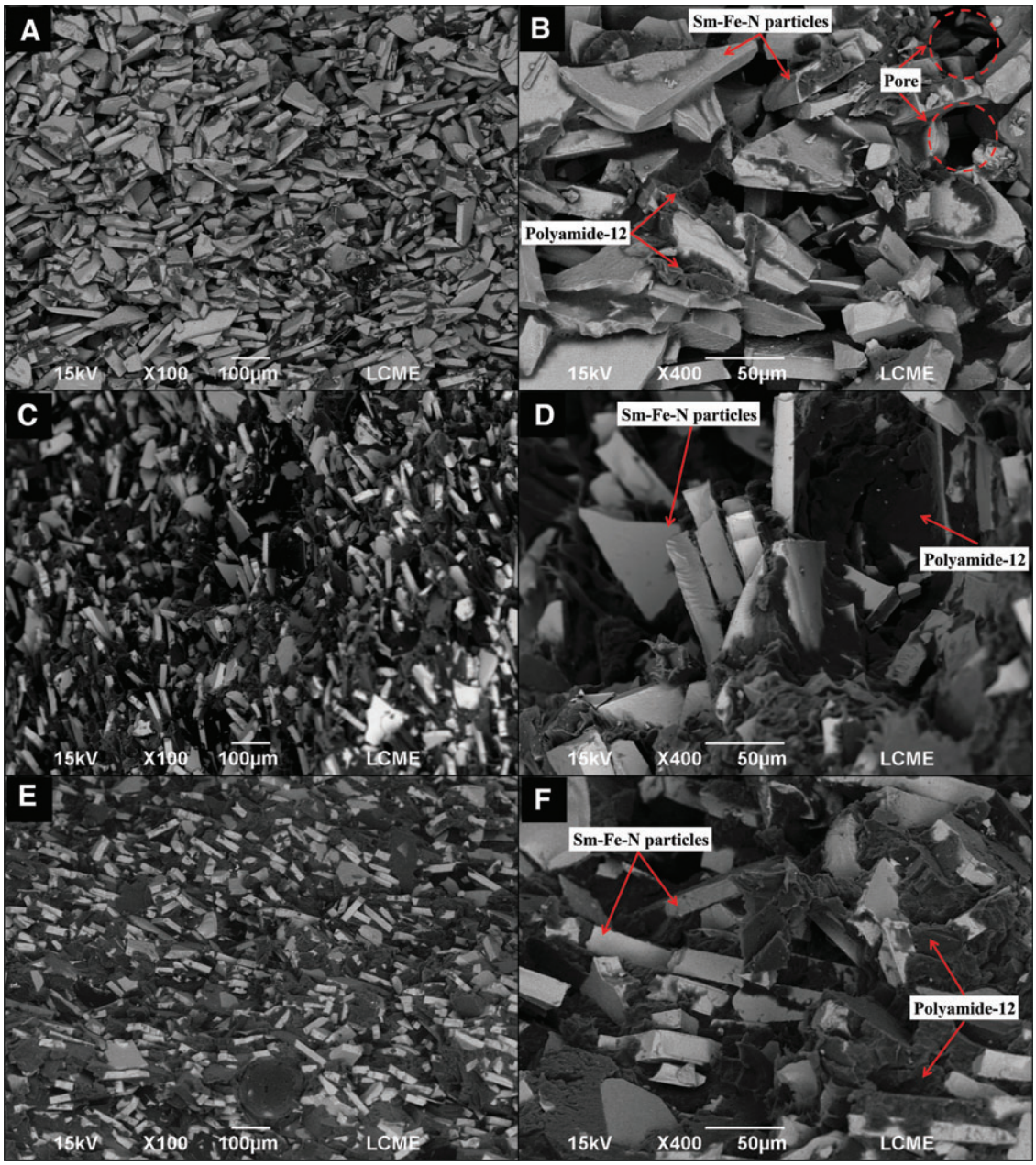

FIG. 3. SEM images from the fracture surface of the as-printed magnetic samples obtained with **(A–B)** 34% vol. PA12, **(C–D)** 60% vol. PA12, and **(E–F)** 65% vol. PA12.

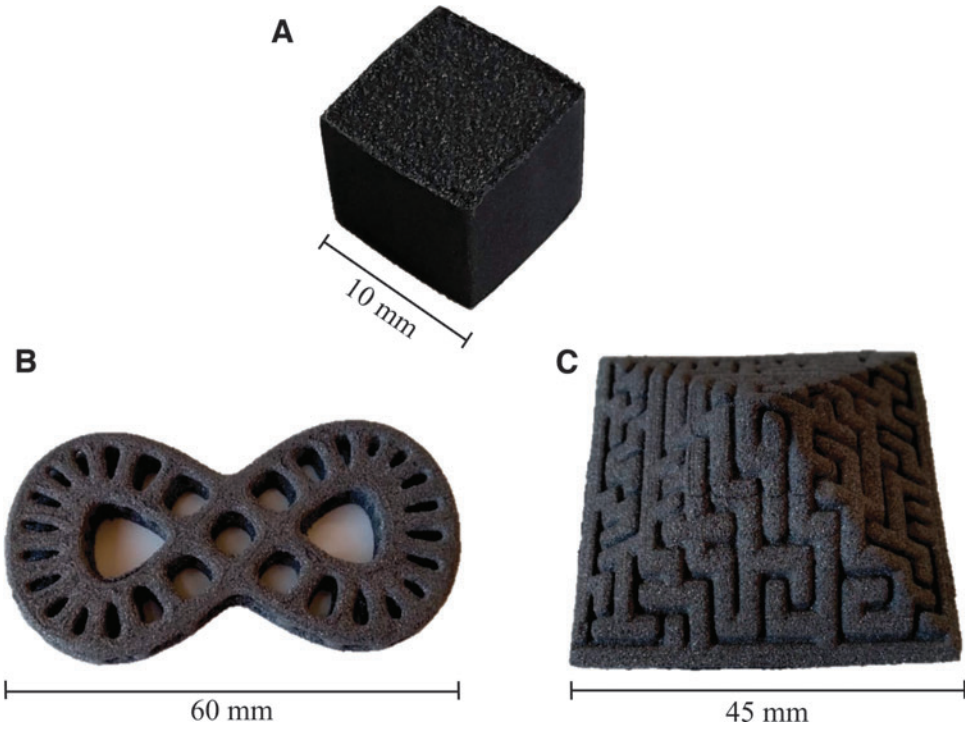

FIG. 4. Examples of as-printed magnetic samples obtained *via* LPBF using 65% vol. of PA12. **(A)** Cubic samples used in this investigation, **(B, C)** nonconventional geometries. LPBF, laser powder bed fusion.

Figure 4 presents examples of (A) cubic as-printed magnetic samples used in this investigation, and (B, C) of non-conventional geometries obtained using the optimized composition described in this work. These samples were produced only for exhibition purposes, aiming to present the capabilities of the technique to produce complex-shaped geometries.

Magnetic measurements

Figure 5 presents the demagnetization curves for the as-printed magnetic samples for each feedstock composition, and the magnetic properties are summarized in Table 4. Only the as-printed samples that exhibited the highest geometrical density values of each batch were selected for this step.

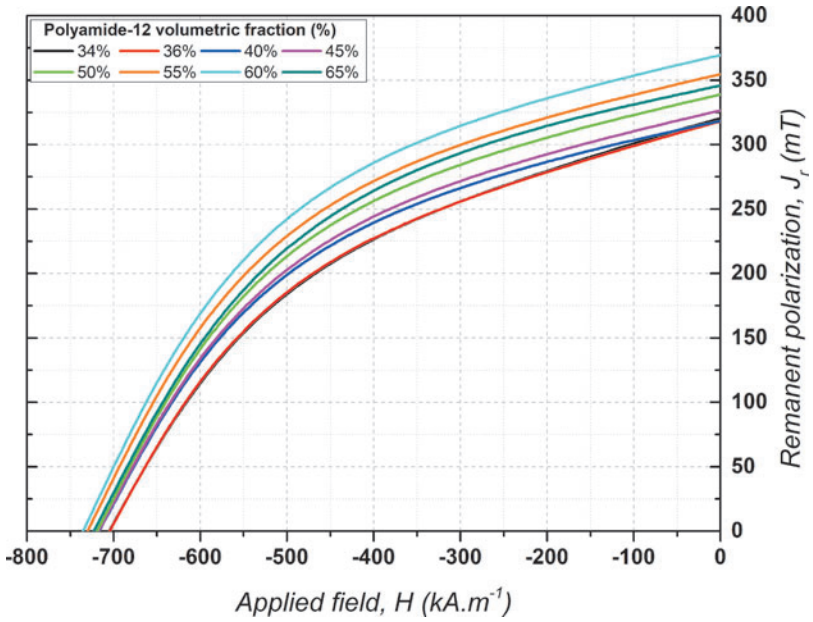

FIG. 5. Demagnetization curves from the as-printed magnetic samples obtained with different PA12 volumetric fractions.

TABLE 4. MAGNETIC PROPERTIES OF THE AS-PRINTED SAMPLES FOR EACH PA12 VOLUMETRIC FRACTION

PA12 fraction (vol.%)	J_r *(mT)*	H_{cj} *(kA.m^{-1})*	$(BH)_{max}$ *(kJ.m^{-3})*
34	320	705	17.6
36	318	705	17.4
40	318	716	18
45	326	717	18.7
50	338	719	20.2
55	354	730	22.1
60	369	735	24
65	345	723	21.3

Remanent polarization (J_r) values increased systematically as the porosity degree was reduced, starting from $J_r = 320$ mT for the interval between 34% and 40% vol. of PA12, reaching a maximum of $J_r = 369$ mT for 60% vol. of PA12 and then decreasing with further polyamide additions ($J_r = 345$ mT for 65% vol. of PA12).

This behavior was expected since some magnetic properties are proportional to the volumetric fraction of magnetic material within the magnet.[22] As seen in Eq. (2), J_r is proportional to the intrinsic properties of the magnetic phase (saturation polarization, J_s) and the extrinsic properties of the as-printed magnets, such as relative density (ρ_{rel}), volumetric fraction of magnetic particles (f), and alignment degree of magnetic particles ($<\cos\theta>$, $\theta = 0$–$90°$).[22]

In this case, since the as-printed magnetic samples are isotropic (i.e., $<\cos\theta> = 0.5$), the variations on J_r values are mainly from porosity-level contributions.[22]

$$J_r = <\cos\theta> \times f \times \rho_{rel} \times J_s \quad (2)$$

In the interval between 34% and 40% vol. PA12, the J_r values were very alike, due to a similar porosity degree ranging from 56% to 48%, as previously shown in Table 3. In this binder fraction interval, the porosity is still elevated and occupies a larger volume than the magnetic particles, causing a reduction in J_r values. As the porosity level decreases, the fraction of magnetic particles within the magnets' volume starts to increase, leading to enhancements on J_r values, as seen on the interval 45% and 55% vol. PA12. In this range, the porosity was reduced from 42% to 26%.

Further increments on polyamide content up to 60% vol. lead to a condition where J_r reached a maximum, with the porosity around 11%. In this optimum point, there is a combination between maximum magnetic particle fraction and minimum porosity achievable, resulting in the highest overall magnetic properties.

Remanent polarization started to decrease from this optimum point with further binder additions, as seen when polyamide content increases to 65% vol. Despite the porosity being reduced to only 3% for this feedstock composition, the reduction in J_r values indicated an excess of the binder. A plot of J_r values as a function of porosity of the as-printed magnets is shown in Figure 6.

Considering that the as-printed magnetic samples present the same volumetric ratio of PA12/Sm-Fe-N as the feedstock, it is possible to estimate the final magnetic particle fraction on the obtained magnets as a function of porosity level. Table 5 summarizes the estimations of Sm-Fe-N powder volume (f) and of the maximum remanence (J_{rmax}) from the as-printed magnets obtained for each feedstock composition.

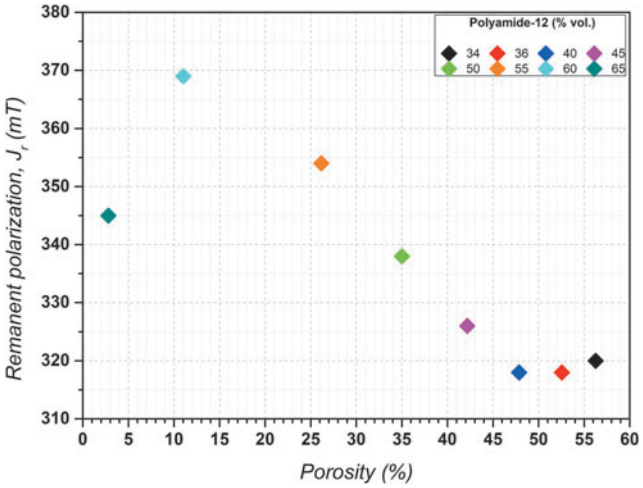

FIG. 6. Remanent polarization (J_r) values of the magnetic samples as function of porosity degree.

For the samples obtained using the ratio 34/66 (34% vol. PA12), the resultant microstructure was only 44% dense (56% of pores). Thus, the consolidated part is composed of 66% vol. of magnetic particles, which represents a final magnetic fraction of 29% vol.

When the ratio 65/35 (65% vol. PA12) was used, the bonded magnets exhibited a microstructure that was 97% consolidated (3% of pores). This consolidated microstructure is then consequently composed by 35% vol. Sm-Fe-N, which results in a final fraction estimated at 34% vol. of magnetic particles.

The ratio 60/40 (60% vol. PA12) generated as-printed magnets with 89% of its microstructure dense (11% porosity). In a similar manner, the final volumetric fraction of magnetic particles was estimated at 36% vol., which is the highest among all explored conditions, in accordance with magnetic measurements.

TABLE 5. SM-FE-N POWDER FRACTION (f) AND MAXIMUM REMANENCE (J_{rmax}*) ESTIMATIONS OF THE AS-PRINTED MAGNETIC SAMPLES OBTAINED FOR EACH FEEDSTOCK COMPOSITION

PA12 fraction (vol.%)	*Porosity, 100-ρ_{rel} (%)*	*Estimated Sm-Fe-N fraction, f (vol. %)*	*Measured J_r (mT)*	*Estimated J_{rmax}* (mT)*
34	56 ± 1.9	29	320	640
36	53 ± 2.5	30	318	620
40	48 ± 0.3	31	318	585
45	42 ± 0.8	32	326	533
50	35 ± 1.9	32	338	485
55	26 ± 2.3	33	354	437
60	11 ± 0.7	36	369	388
65	3 ± 0.8	34	345	339

*J_{rmax} = Sm-Fe-N fraction (f) × powder remanence (970 mT).

This ''trade-off'' relationship between magnetic properties and feedstock composition could be further optimized by adequating the Sm-Fe-N particle morphology to increase its technological properties, such as apparent density values, for example, reducing the necessity of elevated binder fractions to promote proper consolidation.

Apart from porosity elimination, another approach to increase the values of J_r and $(BH)_{max}$ is to develop methods for magnetic alignment of the as-printed parts (increase $< \cos \theta >$ values). Recently, this approach was reported by Gandha *et al.*,[23] where the as-printed magnetic samples obtained *via* extrusion-based AM were magnetically aligned in a post-processing step. The combination of porosity elimination techniques and methods to induce magnetic texture is essential in increasing the performance of the as-printed bonded magnets obtained *via* LPBF.

The intrinsic coercivity (H_{cj}) values systematically increased with porosity reduction, ranging from 705 kA/m (56% porosity) to 735 kA/m (11% porosity). This can be attributed to Sm-Fe-N particle adhesion to the polymeric matrix, where the particle mobility diminishes as the consolidation is enhanced (pore elimination). A similar effect has been reported in previous works.[13,15]

Conclusions

The present work reports the influence of the binder content on the densification process and on the resultant magnetic and microstructural properties of Sm-Fe-N bonded magnets obtained *via* LPBF. The porosity of the as-printed magnetic samples was successfully reduced from 56% to only 3% by increasing the PA12 fraction up to 65% vol., resulting in as-printed magnetic samples with $\rho = 3.32$–$3.35\ g/cm^3$. SEM images revealed the formation of a continuous polymeric matrix only when the binder fraction was ranging between 60% and 65% vol., absent on the other explored conditions. Magnetic measurements at room temperature revealed that this optimization on the consolidation process resulted in an increase on the overall magnetic properties, reaching a maximum for 60% vol. binder, where $J_r = 369$ mT, $H_{cj} = 735$ kA/m, and $(BH)_{max} = 24\ kJ/m^3$.

These results showed that the magnetic performance can be increased as the polymer volumetric fraction is increased to a certain point and can be further optimized with the magnetic particle morphology adequation, leading to a reduction on the binder fractions required to obtain the same densification level.

Acknowledgments

The authors thank LCME-UFSC (LCMEMAT-2021) for the technical support during electron microscopy work. They also thank Daido Electronic, Inc.

Author Disclosure Statement

No competing financial interests exist.

Funding Information

This work was supported by CNPq (project no. 14/50887-4) and CAPES (88882.345177/2014-01).

References

1. Compton BG, Camp JW, Novikov TV, *et al.* Direct-write 3D printing of NdFeB bonded magnets. Mater Manuf Process 2016;;109–113.
2. Huber C, Abert C, Bruckner F, *et al.* 3D print of polymer bonded rare-earth magnets, and 3D magnetic field scanning with an end-user 3D printer. Appl Phys Lett 2016;
3. Paranthaman MP, Shafer CS, Elliott AM, *et al.* Binder jetting: A novel NdFeB bonded magnet fabrication process. JOM 2016;;1978–1982.
4. Shen A, Bailey CP, Ma AWK, *et al.* UV-assisted direct write of polymer-bonded magnets. J Magn Magn Mater 2018;;220–225.
5. Li L, Tirado A, Conner BS, *et al.* A novel method combining additive manufacturing and alloy infiltration for NdFeB bonded magnet fabrication. J Magn Magn Mater 2017;;163–167.
6. Li L, Tirado A, Nlebedim IC, *et al*. Big area additive manufacturing of high performance bonded NdFeB magnets. Sci Rep 2016;:36212.
7. Jaćimović J, Binda F, Herrnann LG, *et al.* Net shape 3D printed NdFeB permanent magnet. Adv Eng Mater 2017;;1–7.
8. Li L, Jones K, Sales B, *et al.* Fabrication of highly dense isotropic Nd-Fe-B nylon bonded magnets via extrusion-based additive manufacturing. Addit Manuf 2018;;495–500.
9. Gandha K, Li L, Nlebedim IC, *et al.* Additive manufacturing of anisotropic hybrid NdFeB-SmFeN nylon composite bonded magnets. J Magn Magn Mater 2018;: 8–13.
10. Tian J, Tang Z, Zuo Z, *et al.* Architecturing high magnetic properties of NdFeB/SmFeN hybrid magnets. Mater Lett 2013;:87–89.
11. Katter M, Wecker J, Schultz L. Structural and hard magnetic properties of rapidly solidified Sm–Fe–N. J Appl Phys 1991;:3188–3196.
12. Coey JMD, Stamenov P, Porter SB, *et al.* Sm-Fe-N revisited; remanence enhancement in melt-spun Nitroquench material. J Magn Magn Mater 2019;:186–192.
13. Engerroff JAB, Baldissera AB, Magalhães MD, *et al.* Additive manufacturing of Sm-Fe-N magnets. J Rare Earths 2019;:1078–1082.
14. Baldissera AB, Pavez P, Wendhausen PAP, *et al.* Additive manufacturing of bonded Nd–Fe–B—Effect of process parameters on magnetic properties. IEEE Trans Magn 2017;:1–4.
15. Fim RGT, Mascheroni AA, Antunes LF, *et al.* Increasing packing density of additively manufactured Nd-Fe-B bonded magnets. Addit Manuf 2020;:1–7.
16. Mapley M, Pauls JP, Tansley G, *et al.* Selective laser sintering of bonded magnets from flake and spherical powders. Scr Mater 2019;:154–158.
17. Van der Schueren B, Kruth JP. Powder deposition in selective metal powder sintering. Rapid Prototyp J 1995;:23–31.
18. White HE, Walton SF. Particle packing and particle shape. J Am Ceram Soc 1937;:155–166.
19. Benesovski F. Fundamental Principles of Powder Metallurgy. London: Edward Arnold Publishers Ltd, 1960;p. 54.
20. Kruth J, Mercelis P, Van Vaerenbergh F. Binding mechanisms in selective laser sintering and selective laser melting. Rapid Prototyp J 2005;:26–36.

21. Gibson I, Rosen D, Stucker B. Powder bed fusion processes. In: Additive Manufacturing Technologies. New York: Springer, 2015; pp. 107–145.
22. McCurrie RA. Determination of the degree of easy axis alignment in uniaxial permanent magnets from remanence measurements. J Appl Phys 1981;:7344–7346.
23. Gandha K, Paranthaman MP, Sales BC, *et al.* 3D printing of anisotropic Sm–Fe–N nylon bonded permanent magnets. Eng Rep 2021;3:e12478.

Address correspondence to:
Melissa Röhrig
Mechanical Engineering Department
Federal University of Santa Catarina
Florianopolis 88040-001
Brazil

E-mail: melissa.rohrig@posgrad.ufsc.br